Journal of Pharmaceutical Analysis 13 (2023) 1296–1308

Contents lists available at ScienceDirect

Journal of Pharmaceutical Analysis

journal homepage: www.elsevier.com/locate/jpa

Original article

Ginsenoside Rg5 enhances the radiosensitivity of lung adenocarcinoma via reducing HSP90-CDC37 interaction and promoting client protein degradation

Hansong Bai [a, 1], Jiahua Lyu [a, b, 1], Xinyu Nie [c], Hao Kuang [a], Long Liang [a], Hongyuan Jia [a], Shijie Zhou [d, **], Churong Li [a, 1, ***], Tao Li [a, b, *]

[a] Sichuan Cancer Hospital Institute, Sichuan Cancer Center, School of Medicine, University of Electronic Science and Technology of China, Chengdu, 610041, China
[b] School of Medicine, University of Electronic Science and Technology of China, Chengdu, 610054, China
[c] School of Clinical Medicine, Southwest Medical University, Luzhou, Sichuan, 646000, China
[d] State Key Laboratory of Biotherapy and Cancer Center/Collaborative Innovation Center for Biotherapy, West China Hospital, Sichuan University, Chengdu, 610041, China

ARTICLE INFO

Article history:
Received 15 March 2023
Received in revised form
2 June 2023
Accepted 5 June 2023
Available online 7 June 2023

Keywords:
Ginsenoside Rg5
Lung adenocarcinoma
Radiotherapy
HSP90
CDC37

ABSTRACT

Ginsenoside Rg5 is a rare ginsenoside showing promising tumor-suppressive effects. This study aimed to explore its radio-sensitizing effects and the underlying mechanisms. Human lung adenocarcinoma cell lines A549 and Calu-3 were used for in vitro and in vivo analysis. Bioinformatic molecular docking prediction and following validation by surface plasmon resonance (SPR) technology, cellular thermal shift assay (CETSA), and isothermal titration calorimetry (ITC) were conducted to explore the binding between ginsenoside Rg5 and 90 kD heat shock protein alpha (HSP90α). The effects of ginsenoside Rg5 on HSP90-cell division cycle 37 (CDC37) interaction, the client protein stability, and the downstream regulations were further explored. Results showed that ginsenoside Rg5 could induce cell-cycle arrest at the G1 phase and enhance irradiation-induced cell apoptosis. It could bind to HSP90α with a high affinity, but the affinity was drastically decreased by HSP90α Y61A mutation. Co-immunoprecipitation (Co-IP) and ITC assays confirmed that ginsenoside Rg5 disrupts the HSP90-CDC37 interaction in a dose-dependent manner. It reduced irradiation-induced upregulation of the HSP90-CDC37 client proteins, including SRC, CDK4, RAF1, and ULK1 in A549 cell-derived xenograft (CDX) tumors. Ginsenoside Rg5 or MRT67307 (an IKKε/TBK1 inhibitor) pretreatment suppressed irradiation-induced elevation of the LC3-II/β ratio and restored irradiation-induced downregulation of p62 expression. In A549 CDX tumors, ginsenoside Rg5 treatment suppressed LC3 expression and enhanced irradiation-induced DNA damage. In conclusion, ginsenoside Rg5 may be a potential radiosensitizer for lung adenocarcinoma. It interacts with HSP90α and reduces the binding between HSP90 and CDC37, thereby increasing the ubiquitin-mediated proteasomal degradation of the HSP90-CDC37 client proteins.

1. Introduction

Non-small cell lung cancers generally include three histologic types, including adenocarcinoma, squamous cell carcinoma, and large cell carcinoma. Lung adenocarcinoma is the most common histologic type [1]. Currently, the treatment of lung cancer is complex and usually involves a variety of strategies, including surgery, radiotherapy, systemic therapy (chemotherapy, immunotherapy, and targeted drugs), interventional radiology, and palliative treatment [2,3]. Radiotherapy is the only treatment with indications in all stages of lung cancer. About 77% of lung cancer patients have evidence-based radiotherapy indications at some

Peer review under responsibility of Xi'an Jiaotong University.
* Corresponding author. Sichuan Cancer Hospital Institute, Sichuan Cancer Center, School of Medicine, University of Electronic Science and Technology of China, Chengdu, 610042, China.
** Corresponding author.
*** Corresponding author.
E-mail addresses: vicjaychou@hotmail.com (S. Zhou), litaoxmf@126.com (T. Li).
[1] These authors contributed equally to this work.

https://doi.org/10.1016/j.jpha.2023.06.004

stage during pathological development [2,3]. However, at the population level, the best radiotherapy regimen can only increase the local control benefit by 8.3% and the survival benefit by 4% in 5-year survival [2,4]. Although radiation technologies have had significant advancements during the past decades, some problems still hinder the therapeutic outcomes of radiotherapies, such as tumor stem cells, tumor heterogeneity, angiogenesis, tumor metabolic changes, and tumor complications [5,6]. A feasible way to overcome these obstacles is to use radiosensitizers [7].

Ginsenosides are active pharmaceutical components [8,9] extracted from the traditional Chinese medicine Ginseng. Ginsenoside Rg5 is a rare ginsenoside that can be absorbed through the intestine [10]. Ginsenoside Rg5 can inhibit transforming growth factor (TGF)-β1-induced epithelial-mesenchymal transformation of human lung adenocarcinoma cells and inhibits the formation of lung cancer stem cells in a dose-dependent manner [11]. In addition, it significantly inhibits TGF-β1-induced matrix metalloproteinase-2/9 activity and activates the Smad2/3 and nuclear factor (NF)-κB/extracellular signal-regulated kinase (ERK) pathways [11]. Overactivated NF-κB/ERK can reduce the radiosensitivity of lung adenocarcinoma [12,13]. Therefore, we speculate that ginsenoside Rg5 may regulate the radiosensitivity of lung adenocarcinoma cells.

Ginsenosides might exert physiological functions via their docking proteins [14]. Our preliminary docking models showed that 90 kD heat shock protein (HSP90) is a potential ginsenoside Rg5 binding protein. HSP90 is a widely expressed molecular chaperone, which promotes the maturation, activation, or stability of its binding/client proteins [15]. More than 300 HSP90 client proteins were identified. Many of them are involved in tumor-related signal pathways and contribute to unlimited growth and resistance to chemotherapy and radiotherapy [15,16].

Therefore, this study aimed to validate the potential radiosensitizing effects of ginsenoside Rg5 in cell-derived xenograft (CDX) lung adenocarcinoma. Then, the interaction between ginsenoside Rg5 and cell division cycle 37 (CDC37) and its influence on the stability and physiological functions of HSP90-CDC37 client proteins were explored.

2. Materials and methods

2.1. Cell culture and treatment

The human non-small-cell lung adenocarcinoma cell lines A549 and Calu-3 were obtained from the American Type Culture Collection (Rockville, MD, USA). Cells were cultured following the protocol introduced previously [17]. Lentiviral particle for HSP90α mutants (E47A (GAG > GCA), Y61A (TAT > GCA), and Q133A (CAG > GCA)) or *ULK1* (NM_003565) overexpression was generated based on pLV-*N*-Flag vector. pLenti-puro-hemagglutinin (HA)-ubiquitin was purchased from Addgene (#74218; Watertown, MA, USA). Lentivirus for infection was produced using the three-plasmid lentivirus production system (recombinant plasmid, pMD2.G, and psPAX2) in HEK293T cells, following the protocol described previously [18]. Cells were infected at a multiplicity of infection of 20, with the presence of 2 μg/mL polybrene. Ginsenoside Rg5 (purity: 99%) was purchased from HerbSubstance (Chengdu, China). It was prepared as a stock solution in dimethyl sulfoxide (DMSO) at 50 mg/mL and placed at −20 °C.

2.2. Reverse transcription quantitative PCR (RT-qPCR)

In brief, total RNAs were extracted and reversely transcribed into complementary DNA (cDNA) using Trizol Reagent (Thermo Fisher Scientific Inc., Waltham, MA, USA) and QuantiTect Reverse Transcription Kit (Qiagen, Venlo, Netherlands), following the manufacturers' instruction. qPCR was conducted with an ABI PRISM 7900HT Sequence Detection System and SYBR Green PCR Master Mix (Thermo Fisher Scientific Inc.). *ULK1* expression was normalized to the expression of *glyceraldehyde-3-phosphate dehydrogenase* (*GAPDH*), using the $2^{-\Delta\Delta CT}$ method. The following primers were used: *ULK1*, forward, 5′-GCAAGGACTCTTCCTGTGACAC-3′; reverse, 5′-CCACTGCACATCAGGCTGTCTG-3′; mouse *GAPDH*, forward, 5′-GTCTCCTCTGACTTCAACAGCG-3′; reverse, 5′-ACCACCCTGTTGCTGTAGCCAA-3′.

2.3. Cell viability assay

Cell viability was measured using Cell Counting Kit (CCK)-8 kit (Beyotime, Shanghai, China) following the manufacturer's instructions. A549 and Calu-3 cells were seeded into 96-well plates (5×10^3 cells/per well). After cell attachment overnight, cells were treated with ginsenoside Rg5 0, 10, 20, 30, 50, 100, 150, and 200 μM) for 48 h. The wells added the same amount of medium is the blank group. Optical density (OD) at 450 nm wavelength was measured with a microplate reader. Each experiment was repeated three times. Cell viability = $[(OD_{Experimental\ group} - OD_{Blank})/(OD_{Control\ group} - OD_{Blank})] \times 100\%$.

2.4. Colony formation assays

A549 or Calu-3 cells were seeded into 24-well plates (500 per well) and were cultured in the medium containing 10, 30, or 60 μM ginsenoside Rg5 for 10 days. Then, the colonies were fixed with 4% (*V*/*V*) methanol and stained with crystal violet. The colonies with over 50 cells were counted. For irradiation-related clonogenic assay, 400 cells were seeded into 24-well plates and incubated 2 h for adhesion. Then, cells were irradiated at defined doses (0, 2, 4, or 6 Gy). After 14 days of incubation, cells were washed, fixed with methanol, and stained with crystal violet. The plating efficiency (PE, the number of colonies formed/the number of cells seeded) of un-irradiated cells was determined before the study, following the protocol introduced previously [19]. Surviving fraction (SF) and survival curves of the irradiated cells were estimated using a linear-quadratic model with the following equation [20]: $Y = \exp(-1 \times (A \times X + B \times X^2))$, in which *Y* is the fraction survival, and *X* is the dose. *A* equals −1 times the initial slope, and the initial value of *B* equals −0.1 times the initial slope.

2.5. Flow cytometric analysis

The proportions of apoptotic cells using Annexin V/propidium iodide (PI) staining, following the protocol introduced previously [21]. Fluorochromes are excited by 488-nm laser, with respective emission peaks detected with a 525 nm for fluorescein isothiocyanate and a 620 nm filter for PI. The stained cells were separated into the following categories: viable cells (annexin V−/PI−), early apoptotic cells (annexin V+/PI−), and late apoptotic or necrotic cells (annexin V+/PI+). The cell-cycle distribution was measured using PI staining alone. After indicating ginsenoside Rg5 treatment for 48 h, cells were harvested, washed in phosphate-buffered saline (PBS), fixed in cold 70% ethanol, and treated with ribonuclease. Then, cells were incubated with PI (30 μg/mL) for 30 min. Flow cytometric analysis was performed using a BD FACSCalibur (BD Bioscience, Franklin Lakes, NJ, USA). Apoptosis and cell-cycle distribution were analyzed using NovoExpress (V.1.5.4, Agilent, Santa Clara, CA, USA).

2.6. Western blot analysis

In brief, cell samples were lysed for protein sample preparation. Then, the samples were measured for protein concentration, separated by sodium dodecyl sulfate-polyacrylamide gel (SDS-

PAGE), and electro-transferred onto nitrocellulose filter membranes (Merck Millipore, Molsheim, Germany). After that, membranes were blocked and incubated with primary antibodies, washed, and incubated with secondary antibodies. Protein band signals were developed by BeyoECL Star Kit (Beyotime) and were captured using a ChemiDoc imaging system (Bio-Rad, Hercules, CA, USA). The antibodies used are provided in Table S1.

2.7. Immunofluorescence assay

The formation of phosphorylated histone variant H2AX (p-γ-H2AX foci) was detected by immunofluorescent staining. A549 and Calu-3 cells were seeded onto culture slides (Corning Inc., Corning, NY, USA). When cells reached about 50% of confluence, cells were pretreated with ginsenoside Rg5 or DMSO for 24 h. Then, cells were subjected to 4 Gy irradiation. Four hours later, the cells were fixed and then permeabilized. The cells were then blocked and incubated with a primary antibody against p-γ-H2AX in a 1:500 dilution overnight at 4 °C. Then, the slides were thoroughly washed and incubated with Alexa Fluor 647-labeled goat anti-rabbit IgG (H+L) in a 1:500 concentration in albumin for 1 h in the dark. The slides were mounted using VECTASHIELD® antifade mounting medium with 4',6-diamidino-2-phenylindole (DAPI). Then, fluorescent images were captured using an FV1000 confocal laser scanning biological microscope (Olympus, Tokyo, Japan).

2.8. Mice and treatment

Animal procedures were approved by the Ethics Committee of Sichuan Cancer Hospital and Institute, China (Approval No.: SCCHEC-04-2020-003). All animal housing and experiments were conducted strictly following the institutional Guidelines for the Care and Use of Laboratory Animals. Animal studies followed the strategies introduced previously [22]. In brief, Nude mice (Balb/C-nude, 5-week-old females) were purchased from Vital River Laboratories (Beijing, China). 5×10^6 A549 cells suspended in a 1:1 mixture of culture media and Matrigel Matrix (Corning Inc., Glendale, AZ, USA) were subcutaneously injected into the lower back. When tumors reached about 200 mm^3, mice were randomly assigned into six groups ($n = 6$ per group). The following six groups were designed: no treatment control, ginsenoside Rg5 (20 mg/kg/day), ginsenoside Rg5 (40 mg/kg/day), irradiation alone (12 Gy, 3 fractions), irradiation + ginsenoside Rg5 (20 mg/kg/day), and irradiation + ginsenoside Rg5 (40 mg/kg/day). Ginsenoside Rg5 was suspended in 0.5% sodium carboxymethylcellulose and was injected intraperitoneally. Irradiation was performed using the X-Rad 320 Biological Irradiator (Precision X-ray, Madison, CT, USA). Mice were anesthetized and shielded with lead. Then the tumors were irradiated at a dose rate of 1.2 Gy/min. Tumor size was measured using calipers every four days. During the treatment and subsequent observation, the long diameter and short diameter of the tumor were monitored every three days. Tumor volume was calculated by $V = l/2 \times$ long diameter $\times$ short diameter^2. When experiments were finished, mice were euthanized using carbon dioxide inhalation, following the American Veterinary Medical Association (AVMA) Guidelines for the Euthanasia of Animals (2020 Edition). Tumor tissues were removed for the following experiments.

2.9. Molecular docking assays to identify the potential docking proteins of ginsenoside Rg5

The potential stigmasterol docking proteins were predicted using SwissTargetPrediction (http://swisstargetprediction.ch/) [23] and TargetNet (http://targetnet.scbdd.com/) [24]. The Protein Data Bank (PDB) format files of HSP90AA1 (1UY6) and HSP90AB1 (1UYM) structures [25] were downloaded from RCSB PDB (https://www.rcsb.org/). The chemical structure of ginsenoside Rg5 was transferred to SMILES chemical format for molecular docking using CB-Dock (http://clab.labshare.cn/cb-dock/php/index.php) [26].

2.10. Cellular thermal shift assay (CETSA)

Cellular thermal shift assay was conducted according to a protocol reported previously [27]. In brief, cells with or without lentiviral-mediated overexpression of Flag-tagged HSP90α mutants (E47A, Y61A, and Q133A) were harvested with PBS buffer and lysed after three freeze-thaw cycles. Then, the cell lysates were mixed and incubated with ginsenosides Rg5 (50 μM) or DMSO (0.1%, *V*/*V*) at room temperature for 30 min. After pre-incubation, the mixture samples were divided into aliquots and submitted to a paralleled incubation at different temperatures ranging from 40 to 70 °C lasting for 5 min. Finally, the denatured samples were centrifuged and subjected to Western blotting assays.

2.11. Surface plasmon resonance (SPR) analysis

The binding affinity of ginsenoside Rg5 to wild-type (WT) or mutant HSP90α proteins were assessed using a Biacore T200 (GE Healthcare, Pittsburgh, PA, USA) following the methods introduced previously [28]. Human recombinant HSP90α protein (AP-160; Novus Biologicals, Littleton, CO, USA) or purified HSP90α mutants (100 μg/mL in 10 mM pH 4.0 sodium acetate) were diluted in sodium acetate buffer and flowed into the CM5 biosensor chip at 10 μL/min for 7 min. Uncoupled protein was washed out by 1 M ethanolamine-HCl (pH 8.0). Binding sensorgrams were recorded by serially injecting diluted ginsenoside Rg5 over the immobilized protein surface. All kinetic constants were estimated using double-subtracted sensorgrams using BiaEvaluation Software (GE Healthcare). The kinetic constants were used to calculate the dissociation constant (K_D), using a single-site bimolecular interaction model (A + B = AB).

2.12. Cloning, expression, and purification of recombinant Hsp90α mutants from Escherichia coli (E. coli)

The cDNA sequence encoding WT (CCDS9967.1) and site-directed mutants (E47A (GAG > GCA), Y61A (TAT > GCA), and Q133A (CAG > GCA)) of Hsp90α were cloned into pET28a respectively, between the NdeI and XhoI restriction sites. Each with an N-terminal 6x-His tag. The recombinant plasmids were transfected into *E. coli* BL21 (DE3) strain, which was then grown in lysogeny broth medium in the presence of ampicillin (100 μg/mL) at 37 °C. When the OD reached about 0.6–0.8, recombinant protein expression was induced via adding isopropyl β-d-1-thiogalactopyranoside at a final concentration of 1 mM for 20 h at 16 °C. Then, the samples were collected via centrifugation at 5,000 rpm for 15 min and stored at −80 °C for use.

Protein purification procedures were performed following the methods introduced previously [29]. In brief, the cells were suspended in lysis buffer and lysed by sonication and further centrifuged at 12,000 rpm for 30 min at 4 °C. Next, the supernatant was filtered using 0.45-μm syringe filters. Then, the lysates were incubated with a Ni-iminodiacetic acid affinity matrix and the protein was eluted with lysis buffer containing 250 mM imidazole. Eluted fractions of Hsp90 proteins were purified by size exclusion chromatography on Superdex 200 columns (Cytiva, Marlborough, MA, USA). All proteins were concentrated and stored in PBS buffer at −80 °C before use.

2.13. Co-immunoprecipitation (Co-IP)

A549 and Calu-3 cells were treated with different concentrations of ginsenoside Rg5 for 48 h. Then, cells were collected,

washed with cold PBS, and lysed with radioimmunoprecipitation assay (RIPA) lysis buffer with protease inhibitors. The lysates were centrifuged to collect the supernatant. 1000 μg proteins were incubated with 2 μg of primary antibodies against HSP90 or CDC37 at 4 °C overnight. Lysates containing protein-antibody complexes were collected using Protein G-agarose beads (Santa Cruz Biotechnology, Santa Cruz, CA, USA) for 6 h at 4 °C. The agarose-bound immunoprecipitated complexes were collected by centrifugation, washed, and then analyzed by Western blotting.

2.14. Isothermal titration calorimetry (ITC)

The influence of ginsenoside Rg5 on the binding affinities between HSP90α (WT and mutants) derived from *E. coli* and CDC37 recombinant protein (NBC1-18377, Novus Biologicals, Centennial, CO, USA) were determined by ITC (MicroCal iTC200, Malvern Panalytical, Westborough, MA, USA). These experiments were conducted at a constant temperature of 15–30 °C. In brief, CDC37 recombinant protein was prepared at 10 μM in assay buffer and loaded into the titration calorimeter cell. The ligand solutions (HSP90α WT or Y61A, with or without the presence of 50 μM ginsenoside Rg5) in syringes were prepared at a concentration of 100 μM in the same assay buffer. Titrations were performed using 25 injections (10 μL each), injected at 3-min intervals. The stirring speed was 500 rpm. All the data obtained from the experiment were analyzed by the Origin software package to determine binding parameters, including the association constant ($K_A = 1/K_D$), enthalpy value (ΔH), and entropy value (ΔS).

2.15. Statistical analysis

Data integration and analysis were conducted using GraphPad Prism 8.1.2 (GraphPad Inc., La Jolla, CA, USA). Welch's unequal variances *t*-test and One-way analysis of variance (ANOVA) with post hoc Tukey's multiple comparisons test were performed for two-group and multiple-group comparisons, respectively. $P < 0.05$ was considered to be statistically significant.

3. Results

3.1. Ginsenoside Rg5 suppresses the proliferation and cell-cycle progression of lung adenocarcinoma

The chemical structure of ginsenoside Rg5 is provided in Fig. 1A. By performing CCK-8 assays, we checked the dose-dependent proliferation suppressive effect of ginsenoside Rg5 on A549 and Calu-3 cells. The half maximal inhibitory concentration (IC_{50}) of ginsenoside Rg5 on A549 and Calu-3 cells are about 68.54 and 84.14 μM, respectively (Figs. 1B and C). Colony formation assays confirmed that ginsenoside Rg5 suppressed colony formation in a dose-dependent manner (Figs. 1D and E). Besides, it inhibited cell-cycle progression by inducing cell-cycle arrest at the G1 phase (Figs. 1F–I). Western blotting assays indicated that ginsenoside Rg5 decreased the expression of p-ERK1/2 and p-signal transducer and activator of transcription 3 (p-STAT3), two signaling proteins critical for tumor cell survival and proliferation (Figs. 1J–L). Ginsenoside Rg5 treatment alone could not induce apoptosis in A549 or Calu-3 cells (Figs. S1A–C). In addition, it did not induce γ-H2AX foci formation (Figs. S1D–F).

3.2. Ginsenoside Rg5 sensitizes lung adenocarcinoma to radiation in vitro and in vivo

Ginsenoside Rg5 increased irradiation (4 Gy)-induced apoptosis (both early and late apoptosis) (Figs. 2A–C) and γ-H2AX foci formation (Figs. 2D–F), and decreased the survival fraction of A549 and Calu-3 cells after irradiation (Figs. 2G and H) in a dose-dependent manner. However, when administered alone, it did not increase the expression of cleaved poly(adenosine diphosphate-ribose) polymerase (PARP) and cleaved caspase-3 but enhanced the expression of these apoptosis-related proteins induced by irradiation (Fig. 2I).

To validate the radio-sensitizing effects of ginsenoside Rg5, we constructed an A549 CDX tumor model on nude mice. The animal study design is summarized in Fig. 3A. After 21 days of implantation of tumor cells, CDX reached about 200 mm^3. For ginsenoside Rg5 treatment, ginsenoside Rg5 (20 or 40 mg/kg) was injected intraperitoneally for three consecutive days. Then the tumor was irradiated using a X-Rad 320 Biological Irradiator (12 Gy, 3 fractions). Ginsenoside Rg5 (20 or 40 mg/kg) was injected intraperitoneally every other day. On the 45th day, the nude mice were euthanized. Tumor tissues were removed and photographed (Fig. 3B). Tumor growth curves showed that ginsenoside Rg5 treatment significantly retarded tumor growth and enhanced the inhibitory effect of irradiation on tumor growth (Fig. 3C). Then, tumor tissues were paraffin-embedded and sectioned for hematoxylin and eosin (H&E), immunohistochemistry, and fluorescence staining. Staining results showed that ginsenoside Rg5 alone suppressed the expression of Ki-67. However, it had limited influence on necrosis (visualized by H&E staining), DNA damage (terminal deoxynucleotidyl transferase dUTP nick-end labeling (TUNEL) positive cells), and the expression of cleaved caspase-3. In comparison, it increased irradiation-induced tumor tissue necrosis, DNA damage, and the expression of cleaved caspase-3. In addition, it enhanced irradiation-induced downregulation of Ki-67 (Fig. 3D).

3.3. Ginsenoside Rg5 interacts with HSP90α with a high affinity

The potential docking proteins of ginsenoside Rg5 were predicted using SwissTargetPrediction and TargetNet. The overlapping candidate set has five proteins, including SLC5A1, HSP90AA1, SLC5A2, PTPN1, and CHRM (Fig. 4A). The chemical structure of ginsenoside Rg5 was transferred to SMILES chemical format for molecular docking. The docking model between ginsenoside Rg5 and HSP90AA1 (HSP90α) was illustrated in Figs. 4B and C. Ginsenoside Rg5 might bind to the N-terminal of HSP90AA1 (Figs. 4B and C). Considering the high level of similarity between HSP90AA1 and HSP90AB1 (HSP90β), we also conducted molecular docking between ginsenoside Rg5 and HSP90AB1. Results confirmed that ginsenoside Rg5 has similar predicted binding positions with HSP90AB1 (the N-terminal) (Fig. S2).

SPR technology was used to verify the binding between ginsenoside Rg5 and the recombinant full-length human HSP90α protein. Results showed that ginsenoside Rg5 could bind to HSP90α with a high affinity ($K_D = 24.83 \pm 1.76$ μM) in a dose-dependent manner (Figs. 4D and K). Then, CETSA was conducted to further validation in cellular samples. 50 μM ginsenoside Rg5 was added to the supernatant of A549 and Calu-3 cell lysates. DMSO was used as a negative control. Western blotting data confirmed that the thermal stability of HSP90 was significantly increased in the groups with ginsenoside Rg5 treatment (Figs. 4E and F).

3.4. Ginsenoside Rg5 reduces the binding between HSP90 and CDC37

CDC37 is a ubiquitous co-chaperone of HSP90 that assists molecular chaperone activity and regulates client proteins in the HSP90 chaperone cycle. The HSP90-CDC37-client interaction plays an essential role in cellular growth and stress response of tumors [30]. Based on one previous publication, we identified the HSP90-CDC37

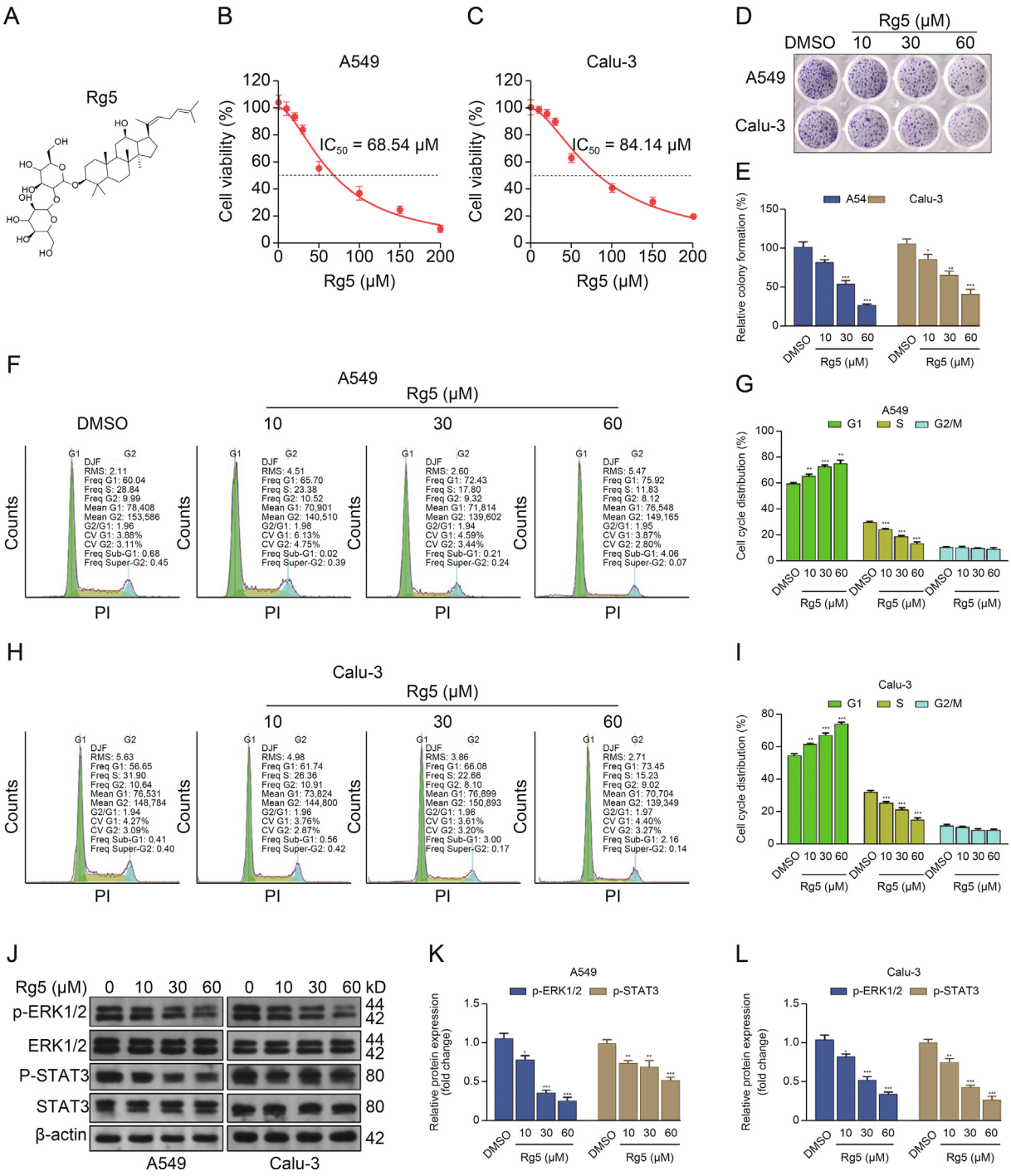

Fig. 1. Ginsenoside Rg 5 (Rg5) suppresses the proliferation and cell-cycle progression of lung adenocarcinoma. (A) The chemical structure of Rg5. (B, C) Cell Counting Kit (CCK)-8 assays were performed to generate the growth suppression curves of different Rg5 doses (0, 10, 20, 30, 50, 100, 150, and 200 μM) on A549 (B) and Calu-3 (C) cells. (D, E) Representative images (D) and quantitation ($n = 3$, E) of colony formation showing the effects of different Rg5 doses (10, 30, and 60 μM) on colony formation of A549 and Calu-3 cells. (F–I) Representative images (F and H) and quantitation ($n = 3$, G and I) of the cell-cycle distribution of A549 and Calu-3 cells after 48 h treatment with different Rg5 doses (10, 30, and 60 μM). (J–L) Representative images (J) and quantitation ($n = 3$, K–L) of the expression of p-extracellular signal-regulated kinase 1/2 (p-ERK1/2), ERK1/2, p-signal transducer and activator of transcription 3 (p-STAT3), and STAT3 in A549 and Calu-3 cells after 48 h treatment with different Rg5 doses (10, 30, and 60 μM). $^{*}P < 0.05$, $^{**}P < 0.01$, and $^{***}P < 0.001$. DMSO: dimethyl sulfoxide; PI: propidium iodide; DJF: Dean-Jett algorithm; RMS: root mean square; Freq: frequency of cells.

binding interface residues, including R46, E47, Y61, S113, K116, A117, E120, A121, A124, A126, M130, Q133, and F134 [29]. Molecular docking data indicated ginsenoside Rg5 might directly interact with the HSP90-CDC37 binding interface residue (Y61) or some nearby residues (G135, V136, G137, F138, and Y139) (Figs. 4B and C). To identify the binding sites between ginsenoside Rg5 and HSP90α in lung adenocarcinoma cells, we generated lentivirus expressing Flag-tagged HSP90α mutant E47A, Y61A, or Q133A for overexpressing in A549 cells. It is known that E47A and Q133A have completely lost binding capability with CDC37, while Y61A has significantly decreased binding affinity [29]. 48 h after lentiviral infection, cellular lysates were applied for CETSA. Results showed that ginsenoside Rg5 significantly increased the thermal stability of HSP90α mutant E47A and Q133A, but not Y61A (Figs. 4G–I), implying that Y61 is a critical site for

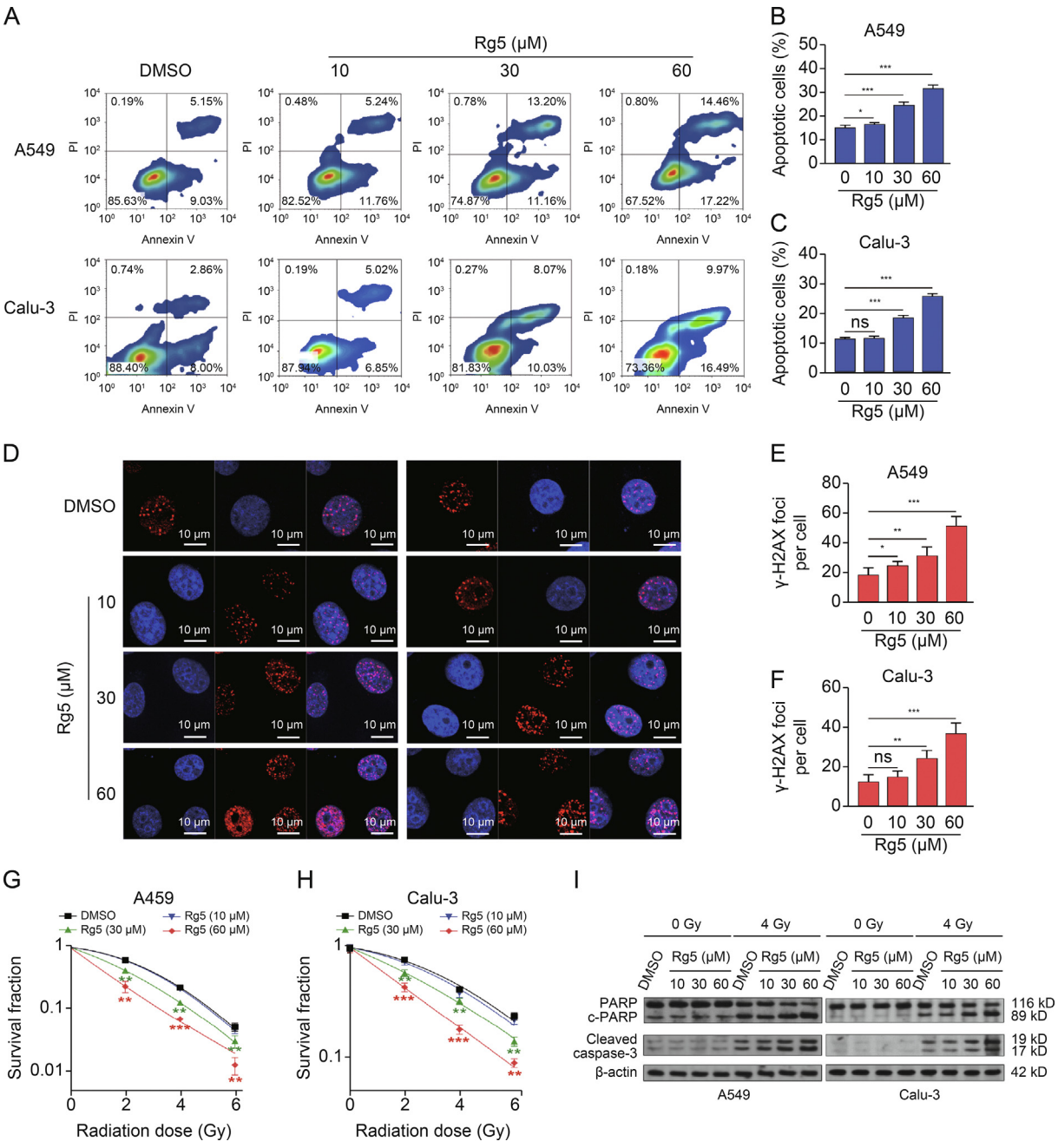

Fig. 2. Ginsenoside Rg 5 (Rg5) sensitizes lung adenocarcinoma to radiation in vitro. (A–C) Rg5 enhanced irradiation-induced apoptosis. A549 and Calu-3 cells were pretreated with Rg5 (10, 30, and 60 μM) for 48 h, and then irradiated (4 Gy). 72 h after irradiation, cell apoptotic death events were determined by flow cytometric analysis of Annexin V/PI staining ($n = 3$). (D–F) Rg5 increased irradiation-induced γ-H2AX foci formation. A549 and Calu-3 cells received the same Rg5 treatment as indicated in Figs. 2A–C. 1 h after irradiation (4 Gy), cells were stained with an anti-γ-H2AX (Ser-139) (red). Nuclei were counterstained with 4',6-diamidino-2-phenylindole (DAPI, blue) (D). The numbers of γ-H2AX foci per cell were quantified (E, F). Each group included 150 cells under 3 different fields. (G, H) Quantitation of clonogenic assay to examine the effects of Rg5 on irradiation (0, 2, 4, and 6 Gy)-induced cell growth suppression of A549 (G) and Calu-3 cells ($n = 3$, H). (I) A549 and Calu-3 cells received the same Rg5 treatment and irradiation, as indicated in Figs. 2A–C. Caspase-3 and poly(adenosine diphosphate-ribose) polymerase (PARP) levels were determined by Western blotting. β-actin was used as an internal control. $^{*}P < 0.05$, $^{**}P < 0.01$, and $^{***}P < 0.001$. DMSO: dimethyl sulfoxide; PI: propidium iodide.

ginsenoside Rg5 binding. To validate these findings, we further conducted SPR assays using purified His-tagged recombinant HSP90α mutants (E47A, Y61A, and Q133A) from *E. coli* (Fig. S3A). Results confirmed that Y61A had drastically decreased affinity with ginsenoside Rg5 ($K_D = 232 \pm 34$ μM) compared to WT (Fig. 4K).

Therefore, we infer that ginsenoside Rg5 might disrupt the HSP90-CDC37-client interaction. To validate this hypothesis, we performed Co-IP assays using A549 and Calu-3 cell lysates with or without 30 or 60 μM of ginsenoside Rg5 treatment. IP was performed using anti-HSP90 (Fig. 5A) or anti-CDC37 (Fig. 5B). Co-IP assays confirmed that ginsenoside Rg5 weakened the HSP90-CDC37 interaction (Figs. 5A and B). Then, Co-IP was performed using cell lysate from cells with lentiviral-mediated HSP90α Y61A (Flag-tagged) overexpression (Figs. 5C and D). Results showed that ginsenoside Rg5 had limited influence on the HSP90α Y61A-CDC37 interaction (Figs. 5C and D). By conducting ITC assays using recombinant HSP90α proteins from *E. coli*, we found that the binding affinity of HSP90α WT and Y61A to CDC37 was 2.68 ± 0.43 μM and

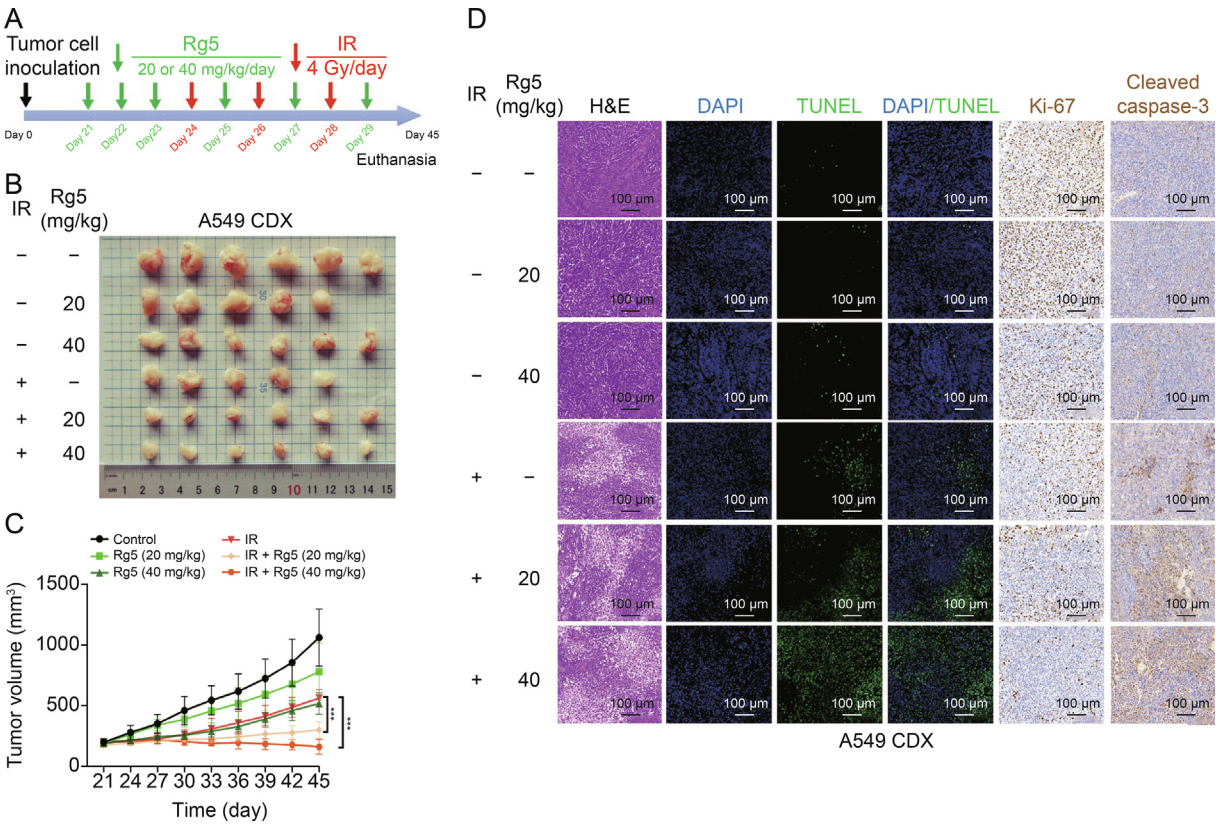

Fig. 3. Ginsenoside Rg 5 (Rg5) sensitizes lung adenocarcinoma to radiation in vivo. (A) A schematic diagram showing the combined Rg5 and irradiation (IR) treatment for A549 cell-derived xenograft (CDX) in nude mice. (B) After the mice were euthanized, the tumors were removed and photographed. (C) The tumor growth curves. (D) Tumor tissues in Fig. 3B were fixed, embedded in paraffin, and sectioned. The tissue sections were used for hematoxylin and eosin (H&E) staining, fluorescence staining for terminal deoxynucleotidyl transferase dUTP nick-end labeling (TUNEL), and immunohistochemical staining for Ki-67 and cleaved caspase-3. $^{***}P < 0.001$. DAPI: 4',6-diamidino-2-phenylindole.

7.59 ± 1.16 μM, respectively (Fig. 5E). Ginsenoside Rg5 had no binding with CDC37. However, pretreatment with ginsenoside Rg5 significantly decreased the affinity of HSP90α WT to CDC37 (34.36 ± 4.92 μM) but did not alter the binding affinity of HSP90α Y61A to CDC37 (8.23 ± 0.79 μM) (Fig. 5E).

Disrupting the HSP90-CDC37 interaction can prevent the association of client protein with HSP90 and suppress protein maturation, leading to proteasomal degradation of client proteins [30]. Therefore, we checked the expression of some HSP90 client proteins using CDX tissues in Fig. 3B. These proteins play important roles in regulating the radiosensitivity of lung adenocarcinoma, including SRC, CDK4, RAF1, and ULK1 (Fig. 5F). Western blotting data showed that p-ERK1/2 expression was suppressed by ginsenoside Rg5 in tumors with or without irradiation treatment (Fig. 5F). The expression of SRC, CDK4, RAF1, and ULK1 was elevated in irradiated tumors (Fig. 5F). However, these trends were reversed by ginsenoside Rg5 treatment (Fig. 5F). The alterations of CDK4 and ULK1 were confirmed by immunohistochemistry staining (Fig. 5G).

3.5. Ginsenoside Rg5 promotes CDK4 and ULK1 degradation via enhancing poly-ubiquitination

Cycloheximide chase assays showed that ginsenoside Rg5 treatment decreased the half-life of ULK1 (Figs. 6A–C) and CDK4 (Figs. 6D–F). To validate the regulatory effects of ginsenoside Rg5 on HSP90 client protein poly-ubiquitination, we used A549 and Calu-3 cells for selective overexpression of HA-ubiquitin. The ubiquitination of CDK4 and ULK1 was checked after IP using an anti-CDK4 or anti-ULK1. Cell samples with ginsenoside Rg5 treatment had a higher level of high molecular-weight smeared bands of CDK4 and ULK1 (Figs. 6G and H), suggesting increased CDK4 and ULK1 poly-ubiquitination.

3.6. Ginsenoside Rg5 reduces irradiation-induced autophagy via reducing ULK1

ULK1 has been characterized as a critical modulator of autophagy [31,32]. In addition, autophagy can enhance the radioresistance of non-small cell lung cancer [33,34]. Therefore, we checked whether the radio-sensitizing effect of ginsenoside Rg5 is partially related to its inhibiting effect on ULK1-mediated autophagy. Autophagosome formation was checked via enforced expression of enhanced green fluorescent protein-microtubule-associated proteins 1A/1B light chain 3B (EGFP-LC3) in A549 and Calu-3. Irradiation increased autophagosome formation. However, the emergence of autophagosomes was significantly weakened by ginsenoside Rg5 or MRT67307 (a selective ULK1 inhibitor) pretreatment (Fig. 7A). Western blotting data confirmed that ginsenoside Rg5 or MRT67307 pretreatment suppressed irradiation-induced elevation of the LC3-II/β ratio and restored irradiation-induced downregulation of p62 expression (Figs. 7B and C). *ULK1* overexpression (Fig. S3B) exacerbated irradiation-induced-induced autophagy (Figs. 7D and E). However, these trends were largely reversed by ginsenoside Rg5 or MRT67307 pretreatment (Figs. 7D and E).

Using A549 CDX tissues, we checked the influence of ginsenoside Rg5 on irradiation-induced autophagy and DNA damage. Results showed that the tumor tissue area with upregulated LC3

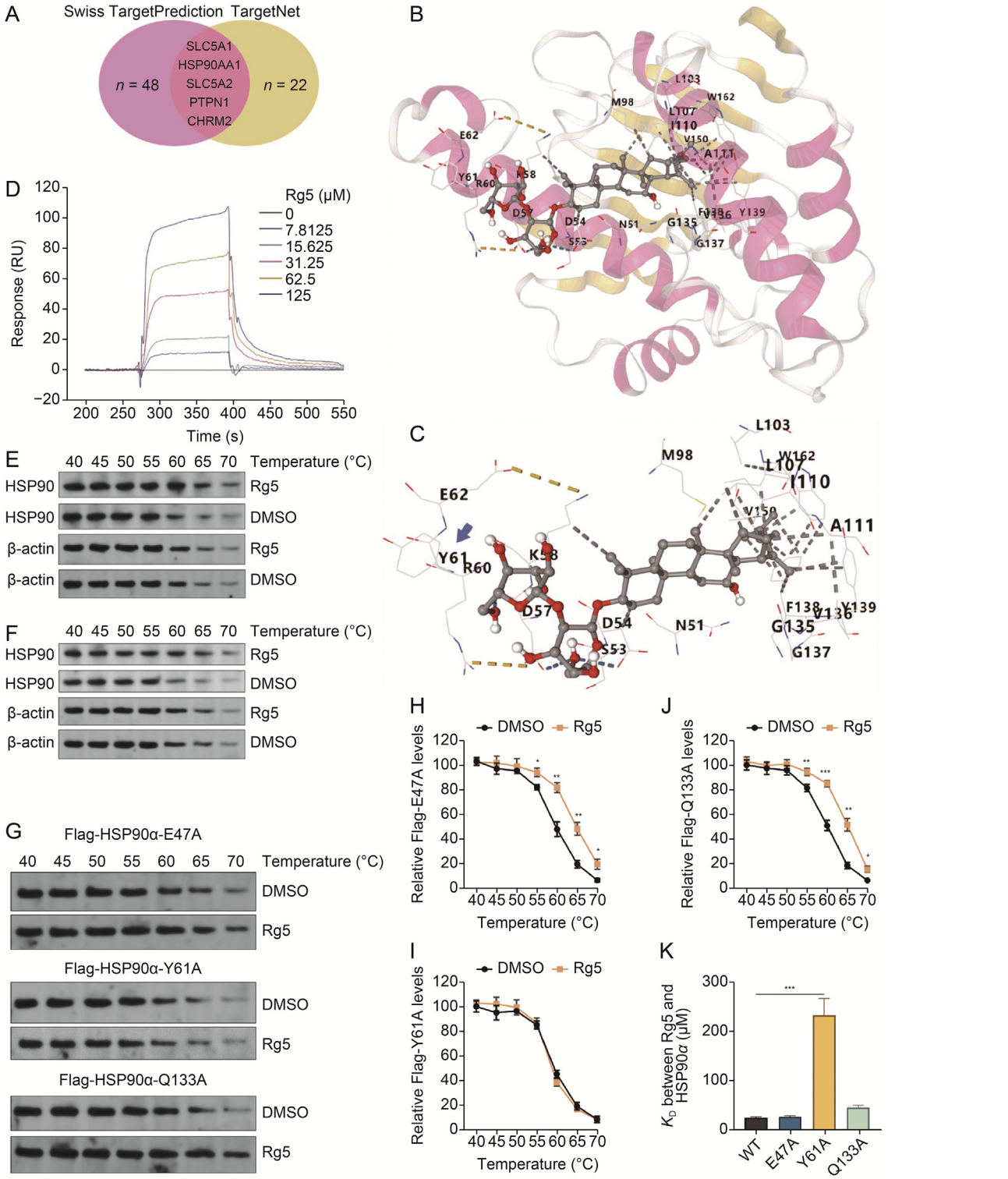

Fig. 4. Ginsenoside Rg 5 (Rg5) interacts with 90 kD heat shock protein alpha (HSP90α). (A) Predict the potential binding proteins of Rg5, using SwissTargetPrediction and TargetNet. (B, C) CB-Dock was used to visualize the binding sites between Rg5 and HSP90α. The docking position of Rg5 within HSP90α (B) and the specific binding sites (C) were provided. (D) Surface plasmon resonance (SPR) analysis was conducted to identify the binding of Rg5 to recombinant human HSP90α protein from *Escherichia coli* (*E. coli*). (E, F) Cellular thermal shift assay (CETSA) experiment was conducted to analyze the effect of Rg5 on the thermostability of HSP90 protein extracted from A549 (E) and Calu-3 (F) cells. Dimethyl sulfoxide (DMSO) was used as a negative control. β-actin was determined as a loading control. (G–J) CETSA experiment was conducted to analyze the effect of Rg5 on the thermostability of Flag-tagged HSP90 mutants (E47A, Y61A, and Q133) overexpressed in A549 cells. HSP90 mutants were detected using anti-Flag tag. Quantitation ($n = 3$, H–J) was conducted to compare the concentration of remaining Flag-tagged proteins. The protein concentration in the DMSO group with 40 °C treatment was set to 100%. (K) Comparison of the affinity between Rg5 and wild type (WT) and purified his-tagged HSP90α mutants (E47A, Y61A, and Q133) from *E. coli* by SPR assays ($n = 3$). $^{*}P < 0.05$, $^{**}P < 0.01$, and $^{***}P < 0.001$. K_D: dissociation constant.

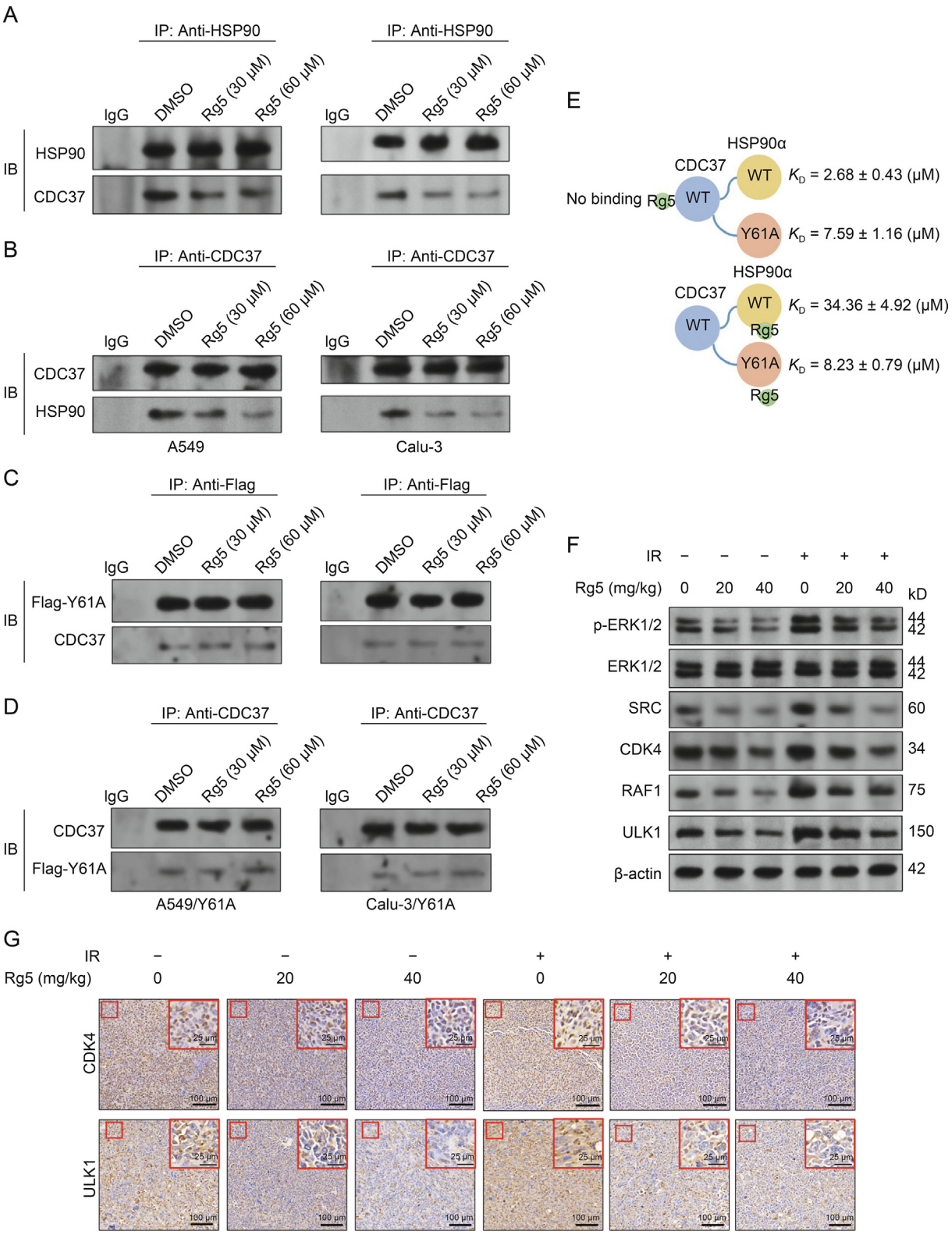

Fig. 5. Ginsenoside Rg 5 (Rg5) reduces the binding between 90 kD heat shock protein (HSP90) and cell division cycle 37 (CDC37). (A, B) A549 and Calu-3 cells were treated with 30 or 60 μM Rg5 for 24 h. Immunoprecipitation (IP) was performed using anti-HSP90 (A) or anti-CDC37 (B). CDC37 precipitated by anti-HSP90 and HSP90 precipitated by anti-CDC37 were detected by Western blotting. (C, D) A549 (left) and Calu-3 (right) cells were infected for lentiviral-mediated HSP90α Y61A (Flag-tagged) overexpression. 48 h later, cells were treated with 30 or 60 μM Rg5 for 24 h. IP was performed using anti-Flag tag (C) or anti-CDC37 (D). CDC37 precipitated by anti-Flag and Flag-tagged HSP90α Y61A (Flag-Y61A) precipitated by anti-CDC37 were detected by Western blotting. (E) Binding affinities of the HSP90α WT or Y61A recombinant proteins (from *Escherichia coli* (*E. coli*)) to CDC37 were determined by isothermal titration calorimetry (ITC). Data are from three independent experiments. (F) Western blotting assays were performed to check the expression of p-extracellular signal-regulated kinase 1/2 (p-ERK1/2), SRC, CDK4, RAF1, and ULK1 in A549 cell-derived xenograft (CDX) tissues in Fig. 3B. (G) Immunohistochemistry staining was performed to check the expression of CDK4 and ULK1 in A549 CDX tissues in Fig. 3B. IB: immunoblotting; DMSO: dimethyl sulfoxide; WT: wild-type; IR: irradiation.

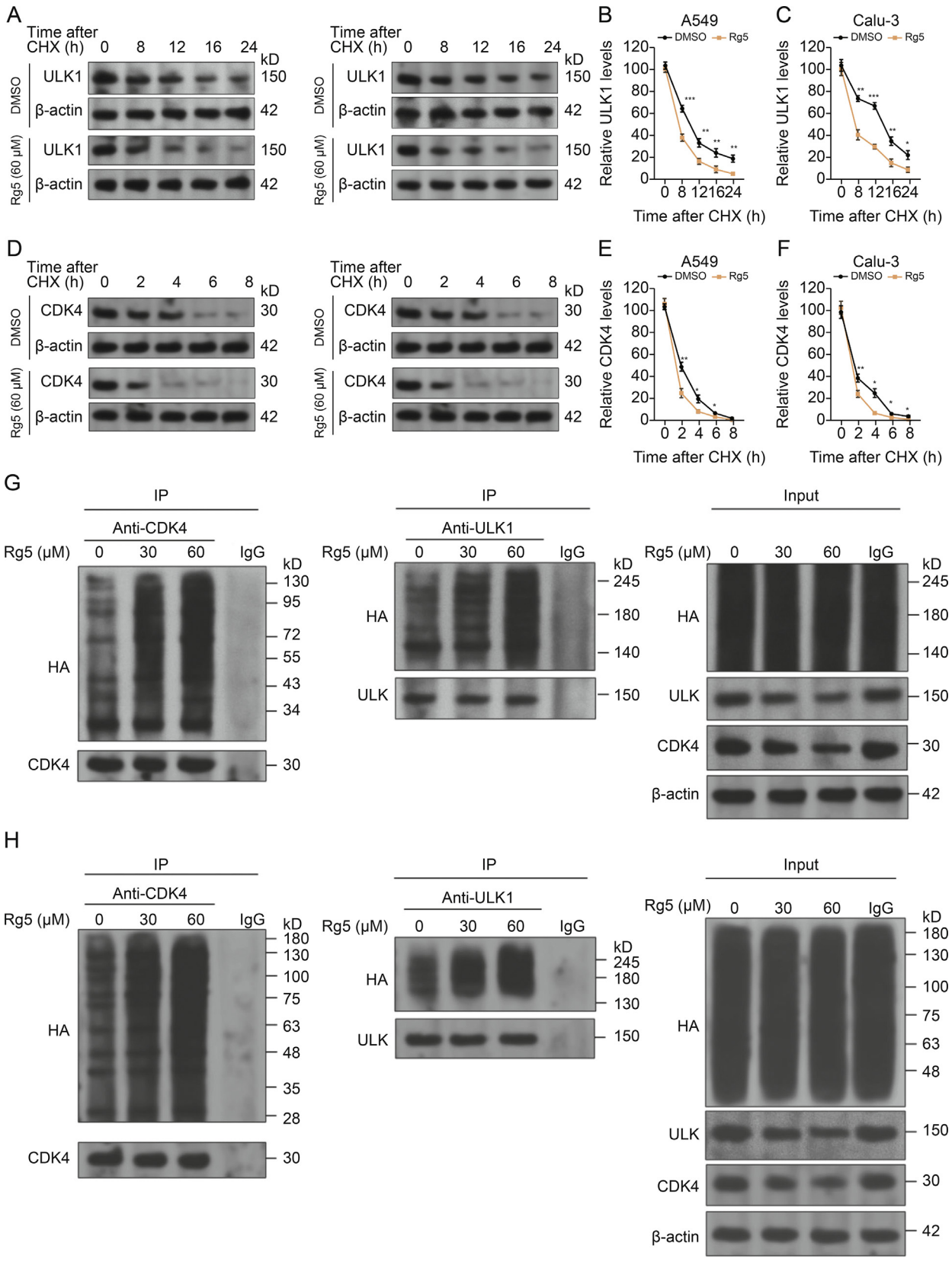

Fig. 6. Ginsenoside Rg 5 (Rg5) promotes CDK4 and ULK1 degradation via enhancing poly-ubiquitination. (A–F) A549 and Calu-3 cells with or without pretreatment of Rg5 (60 μM for 24 h) or dimethyl sulfoxide (DMSO) were incubated in the presence of 20 μM cycloheximide (CHX) for the indicated times ($n = 3$ per group). (A, D) Proteins were then analyzed by Western blotting with the indicated antibodies. Quantitation of the relative levels of ULK1 (B, C) and CDK4 (E, F) were determined from Western blots using the ImageJ software. Data are expressed as mean ± standard deviation. Comparison was performed between the Rg5 and DMSO groups. $^{*}P < 0.05$, $^{**}P < 0.01$, and $^{***}P < 0.001$. (G, H) Western blots of in vitro ubiquitination assay. A549 (G) and Calu-3 (H) cells were infected with pLenti-puro-hemagglutinin (HA)-ubiquitin. 24 h later, cells were treated with Rg5 for another 24 h.

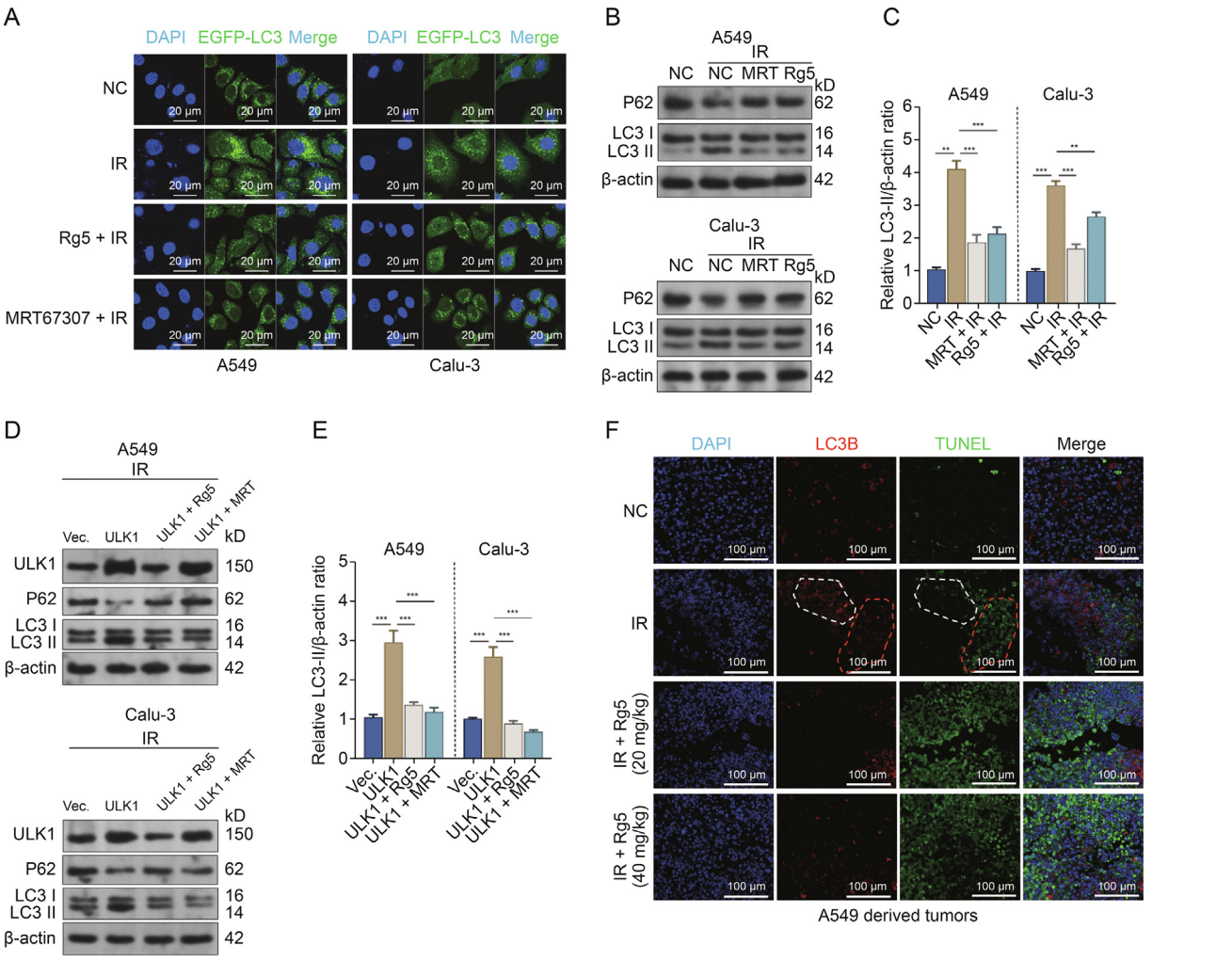

Fig. 7. Ginsenoside Rg 5 (Rg5) reduces irradiation-induced autophagy via reducing ULK1. (A) Formation of LC3 foci in A549 and Calu-3 4 h after irradiation (4 Gy). Cells were either dimethyl sulfoxide (DMSO) treated (negative control (NC)), irradiated, pretreated with Rg5 (60 μM, 24 h) followed by irradiation (IR), or pretreated with MRT67307 (10 μM, 1 h) followed by IR. Cells were fixed and subjected to indirect immunofluorescence analysis. (B) The expression of LC3-I, LC3-II, and p62 in A549 and Calu-3 cells with or without Rg5 (60 μM, 24 h) or MRT67307 (10 μM, 1 h) treatment following irradiation (4 Gy). (C) LC3-II/β-actin ratios in Fig. 7B were quantified using three independent experiments. (D) The expression of LC3-I, LC3-II, and p62 in A549 and Calu-3 cells with *ULK1* overexpression alone, or in combination with Rg5 (60 μM, 24 h) or MRT67307 (10 μM, 1 h) treatment following irradiation (4 Gy). (E) LC3-II/β-actin ratios in Fig. 7D were quantified using three independent experiments. (F) The expression of LC3 and terminal deoxynucleotidyl transferase dUTP nick-end labeling (TUNEL) in representative A549 cell-derived xenograft (CDX) tumors as in Fig. 3B. $^{**}P < 0.01$ and $^{***}P < 0.001$. DAPI: 4',6-diamidino-2-phenylindole; EGFP-LC3: enhanced green fluorescent protein-microtubule-associated proteins 1A/1B light chain 3B; Vec.: vector control; LC3B: microtubule-associated proteins 1A/1B light chain 3B.

expression might have less DNA damage (low TUNEL staining) (Fig. 7F, white dotted area). In comparison, the tumor tissue area without LC3 upregulation is associated with a higher level of DNA damage (Fig. 7F, red dotted area). Ginsenoside Rg5 treatment suppressed LC3 expression and enhanced irradiation-induced DNA damage (Fig. 7F).

4. Discussion

Natural products are easier to store, lower in cost, and with safety more convenient to be evaluated than synthetic chemical drugs [35]. The different effects of natural products on normal and tumor cells/tissues make them potential therapeutic reagents. Recent preclinical and clinical trials revealed that some natural products could attenuate oral mucositis, gastrointestinal toxicity, hepatotoxicity, nephrotoxicity, hematopoietic system damage, cardiac toxicity, and neurotoxicity caused by chemotherapy and radiotherapy [36]. Some natural products, such as ginseng extract, grape seed extract, and curcumin, might exert radio-sensitizing effects in tumor treatment and reduce the damage of ionizing radiation to normal cells/tissues. The tumor-suppressive effects of ginsenoside Rg5 have been demonstrated in multiple cancers, such as hepatocellular cancer [37], breast cancer [38], and esophageal carcinoma [39]. In this study, we found that ginsenoside Rg5 may be a potential radiosensitizer in lung adenocarcinoma. It interacts with HSP90 and reduces the binding between HSP90 and CDC37.

Via inhibiting HSP90, HSP90 client proteins might become unstable and can be rapidly degraded. The signals necessary for tumor cell survival are impaired. Therefore, inhibition of HSP90 is a potential target for tumor therapy [40]. Several preclinical studies confirmed that inhibition of HSP90 can promote the radiosensitivity of lung adenocarcinoma cells [41–43]. Various HSP90 inhibitor compounds are currently being used as a single treatment scheme or in combination with conventional chemotherapy and

Then, cells were lysed, and the cell lysates were subjected to co-immunoprecipitation (Co-IP) assays. IP was conducted using anti-CDK4 (left panels) or anti-ULK1 (middle panels). The right panels are input controls. Co-IP was performed using anti-HA. IR: irradiation.

radiotherapy in preclinical or phase I–III clinical trials [44]. However, so far, at least 18 HSP90 inhibitors have entered clinical trials, but none have been approved for clinical use due to adverse effects, including cardiac, gastrointestinal, and ocular toxicity [40,45].

Looking for potential HSP90 inhibitors from natural products is a feasible direction [40]. Some natural products are potential HSP90 inhibitors, such as platycodon D isolated from traditional Chinese medicine Platycodon grandiflorum, triptolide A isolated from Tripterygium wilfordii, and gambogic acid (−) found in Gamboge [40]. In the current study, we found that ginsenoside Rg5 can disrupt the interaction between HSP90 and CDC37, and then induce the degradation of multiple HSP90 client proteins, including SRC, CDK4, RAF1, and ULK1. Using CDK4 and ULK1 as representative candidates, we showed that ginsenoside Rg5 could promote the degradation of HSP90-CDC37 client proteins via the ubiquitin-mediated proteasomal pathway. Aberrant CDK4 expression is associated with lung adenocarcinoma cell-cycle progression and cell proliferation [46]. Inhibiting CDK4 can prevent cell proliferation through G1 arrest [47]. This mechanism helps explain why ginsenoside Rg5 treatment induces G1 arrest in lung adenocarcinoma cells. Tumor cells at the G1 and G2/M phases are more radiosensitive than their counterparts in the S phase [48]. This might also be one potential mechanism of the radio-sensitizing effects of ginsenoside Rg5.

ULK1 can promote autophagy via phosphorylating Beclin-1 and activating VPS34 lipid kinase [31]. Elevated autophagy has been characterized as an important mechanism of radioresistance in lung cancer [33,34]. Autophagy might be a cytoprotective response supporting tumor cells to conquer survival stress and promote resistance to radiotherapy [49,50]. By checking LC-3 and p62 expression in lung adenocarcinoma cell lines and A549 CDX tissues, we confirmed that ginsenoside Rg5 could reduce irradiation-induced autophagy via reducing ULK1 expression. The findings of the current studies explain not only the radio-sensitizing effects but also the tumor-suppressive mechanisms of ginsenoside Rg5. For instance, ginsenoside Rg5 can inhibit epithelial-mesenchymal transition anoikis resistance and the acquisition of stem-like properties of lung cancer cells [11]. Some HSP90-CDC37 client proteins are related to these properties, such as CDK4 [51] and SRC [52].

Ginsenosides might be absorbed by passive diffusion [53]. Besides, ginsenoside Rg5 might be actively transported via GLUT1 [54], GLUT2, and GLUT5 [55]. Once it enters cells, it might interact with HSP90α and exert physiological regulations. Since lung adenocarcinoma usually has high expression of GLUT1 [56] and GLUT5 [57], ginsenoside Rg5 might have a certain level of tumor targeting effects. Some recent studies revealed that ginsenoside-based (such as ginsenosides Rg3 and Rg5) liposomes have cancer-stem cell targeting and intratumorally diffusion capability [58,59]. Ginsenoside Rg3 or Rg5 can be a stabilizer by inserting into the liposome membrane and interacting with phospholipids [58–60]. In addition, the glucose part of the hydrophilic part of Rg3 will theoretically extend beyond the surface of the liposome, serving as an ideal ligand for glucose transporter 1, which is usually overexpressed in tumors [60]. These modified liposomes carrying chemotherapeutic drugs can capture circulating tumor cells and destroy their metastatic potential [60]. In the future, it is meaningful to develop ginsenoside Rg5 liposomes carrying other radio-sensitizers or chemotherapeutic drugs, as an adjuvant strategy to improve the radiosensitivity of lung adenocarcinoma.

5. Conclusions

Ginsenoside Rg5 may be a potential radiosensitizer for lung adenocarcinoma. It interacts with HSP90α and reduces the binding between HSP90 and CDC37, thereby increasing the ubiquitin-mediated proteasomal degradation of the HSP90-CDC37 client proteins.

CRediT author statement

Hansong Bai: Conceptualization, Investigation, Formal analysis, Validation, Writing - Original draft preparation, Reviewing and Editing; **Jiahua Lyu:** Methodology, Writing - Reviewing and Editing; **Xinyu Nie:** Visualization; **Hao Kuang:** Investigation; **Long Liang:** Formal analysis; **Hongyuan Jia:** Validation; **Shijie Zhou:** Conceptualization, Software; Resources, Data curation; **Churong Li:** Investigation; Writing - Reviewing and Editing, Resources, Supervision; **Tao Li:** Supervision, Funding acquisition, Project administration.

Declaration of competing interest

The authors declare that there are no conflicts of interest.

Acknowledgments

This work was supported by grants from the Project of Sichuan Science and Technology Department, China (Grant No.: 2021YJ0010).

Appendix A. Supplementary data

Supplementary data to this article can be found online at https://doi.org/10.1016/j.jpha.2023.06.004.

References

[1] A.G. Nicholson, M.S. Tsao, M.B. Beasley, et al., The 2021 WHO classification of lung tumors: Impact of advances since 2015, J. Thorac. Oncol. 17 (2022) 362–387.
[2] S.K. Vinod, E. Hau, Radiotherapy treatment for lung cancer: Current status and future directions, Respirology 25 (2020) 61–71.
[3] G.P. Delaney, M.B. Barton, Evidence-based estimates of the demand for radiotherapy, Clin. Oncol. (R. Coll. Radiol.) 27 (2015) 70–76.
[4] J. Shafiq, T.P. Hanna, S.K. Vinod, et al., A population-based model of local control and survival benefit of radiotherapy for lung cancer, Clin. Oncol. (R. Coll. Radiol.) 28 (2016) 627–638.
[5] M. Krause, A. Dubrovska, A. Linge, et al., Cancer stem cells: Radioresistance, prediction of radiotherapy outcome and specific targets for combined treatments, Adv. Drug Deliv. Rev. 109 (2017) 63–73.
[6] S. Rey, L. Schito, M. Koritzinsky, et al., Molecular targeting of hypoxia in radiotherapy, Adv. Drug Deliv. Rev. 109 (2017) 45–62.
[7] H. Wang, X. Mu, H. He, et al., Cancer radiosensitizers, Trends Pharmacol. Sci. 39 (2018) 24–48.
[8] Y. Chen, Q. Liu, P. An, et al., Ginsenoside Rd: A promising natural neuroprotective agent, Phytomedicine 95 (2022), 153883.
[9] Y. Yang, Z. Ju, Y. Yang, et al., Phytochemical analysis of *Panax* species: A review, J. Ginseng Res. 45 (2021) 1–21.
[10] S. Yoo, B.I. Park, D.H. Kim, et al., Ginsenoside absorption rate and extent enhancement of black ginseng (CJ EnerG) over red ginseng in healthy adults, Pharmaceutics 13 (2021), 487.
[11] H. Kim, P. Choi, T. Kim, et al., Ginsenosides Rk1 and Rg5 inhibit transforming growth factor-β1-induced epithelial-mesenchymal transition and suppress migration, invasion, anoikis resistance, and development of stem-like features in lung cancer, J. Ginseng Res. 45 (2021) 134–148.
[12] X. Yang, G. Wang, J. You, et al., High expression of cancer-IgG is associated with poor prognosis and radioresistance via PI3K/AKT/DNA-PKcs pathway regulation in lung adenocarcinoma, Front. Oncol. 11 (2021), 675397.
[13] A. Tsolou, M. Liousia, D. Kalamida, et al., Inhibition of IKK-NFκB pathway sensitizes lung cancer cell lines to radiation, Cancer Biol. Med. 14 (2017) 293–301.
[14] K. Park, A.E. Cho, Using reverse docking to identify potential targets for ginsenosides, J. Ginseng Res. 41 (2017) 534–539.
[15] A.E. Kabakov, V.A. Kudryavtsev, V.L. Gabai, Hsp90 inhibitors as promising agents for radiotherapy, J. Mol. Med. 88 (2010) 241–247.
[16] E. Amatya, B.S.J. Blagg, Recent advances toward the development of Hsp90 C-terminal inhibitors, Bioorg. Med. Chem. Lett. 80 (2023), 129111.
[17] Q. Wang, Y. Chen, H. Chang, et al., The role and mechanism of ATM-mediated autophagy in the transition from hyper-radiosensitivity to induced radioresistance in lung cancer under low-dose radiation, Front. Cell Dev. Biol. 9 (2021), 650819.

[18] J. Elegheert, E. Behiels, B. Bishop, et al., Lentiviral transduction of mammalian cells for fast, scalable and high-level production of soluble and membrane proteins, Nat. Protoc. 13 (2018) 2991–3017.
[19] N.A. Franken, H.M. Rodermond, J. Stap, et al., Clonogenic assay of cells *in vitro*, Nat. Protoc. 1 (2006) 2315–2319.
[20] L. Bodgi, N. Foray, The nucleo-shuttling of the ATM protein as a basis for a novel theory of radiation response: Resolution of the linear-quadratic model, Int. J. Radiat. Biol. 92 (2016) 117–131.
[21] I. Lakshmanan, S.K. Batra, Protocol for apoptosis assay by flow cytometry using annexin V staining method, Bio. Protoc. 3 (2013), e374.
[22] Q. Song, J. Wen, W. Li, et al., HSP90 promotes radioresistance of cervical cancer cells via reducing FBXO6-mediated CD147 polyubiquitination, Cancer Sci. 113 (2022) 1463–1474.
[23] A. Daina, O. Michielin, V. Zoete, SwissTarget Prediction: Updated data and new features for efficient prediction of protein targets of small molecules, Nucleic Acids Res. 47 (2019) W357–W364.
[24] Z. Yao, J. Dong, Y. Che, et al., TargetNet: A web service for predicting potential drug-target interaction profiling via multi-target SAR models, J. Comput. Aided Mol. Des. 30 (2016) 413–424.
[25] L. Wright, X. Barril, B. Dymock, et al., Structure-activity relationships in purine-based inhibitor binding to HSP90 isoforms, Chem. Biol. 11 (2004) 775–785.
[26] Y. Liu, M. Grimm, W. Dai, et al., A web server for cavity detection-guided protein-ligand blind docking, Acta Pharmacol. Sin. 41 (2020) 138–144.
[27] C. Zhou, C. Zhang, H. Zhu, et al., Allosteric regulation of Hsp90α's activity by small molecules targeting the middle domain of the chaperone, iScience 23 (2020), 100857.
[28] D. Raghu, P. Hamill, A. Banaji, et al., Assessment of the binding interactions of SARS-CoV-2 spike glycoprotein variants, J. Pharm. Anal. 12 (2022) 58–64.
[29] L. Wang, L. Zhang, L. Li, et al., Small-molecule inhibitor targeting the Hsp90-Cdc37 protein-protein interaction in colorectal cancer, Sci. Adv. 5 (2019), eaax2277.
[30] T. Li, H. Jiang, Y. Tong, et al., Targeting the Hsp90-Cdc37-client protein interaction to disrupt Hsp90 chaperone machinery, J. Hematol. Oncol. 11 (2018), 59.
[31] R.C. Russell, Y. Tian, H. Yuan, et al., ULK1 induces autophagy by phosphorylating Beclin-1 and activating VPS34 lipid kinase, Nat. Cell Biol. 15 (2013) 741–750.
[32] W. Wu, X. Wang, N. Berleth, et al., The autophagy-initiating kinase ULK1 controls RIPK1-mediated cell death, Cell Rep. 31 (2020), 107547.
[33] X. Chen, P. Wang, F. Guo, et al., Autophagy enhanced the radioresistance of non-small cell lung cancer by regulating ROS level under hypoxia condition, Int. J. Radiat. Biol. 93 (2017) 764–770.
[34] H. Chaachouay, P. Ohneseit, M. Toulany, et al., Autophagy contributes to resistance of tumor cells to ionizing radiation, Radiother. Oncol. 99 (2011) 287–292.
[35] S. Nisar, T. Masoodi, K.S. Prabhu, et al., Natural products as chemo-radiation therapy sensitizers in cancers, Biomed. Pharmacother. 154 (2022), 113610.
[36] Q. Zhang, F. Wang, K. Jia, et al., Natural product interventions for chemotherapy and radiotherapy-induced side effects, Front. Pharmacol. 9 (2018), 1253.
[37] L. Yang, X. Zhang, K. Li, et al., Protopanaxadiol inhibits epithelial-mesenchymal transition of hepatocellular carcinoma by targeting STAT3 pathway, Cell Death Dis. 10 (2019), 630.
[38] Y. Liu, D. Fan, The preparation of ginsenoside Rg5, its antitumor activity against breast cancer cells and its targeting of PI3K, Nutrients 12 (2020), 246.
[39] Z. Niu, W. Zhang, J. Shi, et al., Effect of silencing C-erbB-2 on esophageal carcinoma cell biological behaviors by inhibiting IGF-1 pathway activation, J. Cardiothorac. Surg. 16 (2021), 194.
[40] M.A. Serwetnyk, B.S.J. Blagg, The disruption of protein-protein interactions with co-chaperones and client substrates as a strategy towards Hsp90 inhibition, Acta Pharm. Sin. B 11 (2021) 1446–1468.
[41] T.T. Koll, S.S. Feis, M.H. Wright, et al., HSP90 inhibitor, DMAG, synergizes with radiation of lung cancer cells by interfering with base excision and ATM-mediated DNA repair, Mol. Cancer Ther. 7 (2008) 1985–1992.
[42] Y. Wang, H. Liu, L. Diao, et al., Hsp90 inhibitor ganetespib sensitizes non-small cell lung cancer to radiation but has variable effects with chemoradiation, Clin. Cancer Res. 22 (2016) 5876–5886.
[43] M. Provencio, A. Sánchez, P. Garrido, et al., New molecular targeted therapies integrated with radiation therapy in lung cancer, Clin. Lung Cancer 11 (2010) 91–97.
[44] L. Li, L. Wang, Q. You, et al., Heat shock protein 90 inhibitors: An update on achievements, challenges, and future directions, J. Med. Chem. 63 (2020) 1798–1822.
[45] Y. Xiao, Y. Liu, Recent advances in the discovery of novel HSP90 inhibitors: An update from 2014, Curr. Drug Targets 21 (2020) 302–317.
[46] A. Wu, B. Wu, J. Guo, et al., Elevated expression of CDK4 in lung cancer, J. Transl. Med. 9 (2011), 38.
[47] S. Goel, J.S. Bergholz, J.J. Zhao, Targeting CDK4 and CDK6 in cancer, Nat. Rev. Cancer 22 (2022) 356–372.
[48] S. Biade, C.C. Stobbe, J.D. Chapman, The intrinsic radiosensitivity of some human tumor cells throughout their cell cycles, Radiat. Res. 147 (1997) 416–421.
[49] S.Y. Tam, V.W. Wu, H.K. Law, Influence of autophagy on the efficacy of radiotherapy, Radiat. Oncol. 12 (2017), 57.
[50] J. Gao, F. Lu, J. Yan, et al., The role of radiotherapy-related autophagy genes in the prognosis and immune infiltration in lung adenocarcinoma, Front. Immunol. 13 (2022), 992626.
[51] M. Dai, C. Zhang, A. Ali, et al., CDK4 regulates cancer stemness and is a novel therapeutic target for triple-negative breast cancer, Sci. Rep. 6 (2016), 35383.
[52] M.A. Ortiz, T. Mikhailova, X. Li, et al., Src family kinases, adaptor proteins and the actin cytoskeleton in epithelial-to-mesenchymal transition, Cell Commun. Signal. 19 (2021), 67.
[53] S. Gao, H. Kushida, T. Makino, Ginsenosides, ingredients of the root of *Panax ginseng*, are not substrates but inhibitors of sodium-glucose transporter 1, J. Nat. Med. 71 (2017) 131–138.
[54] X. Wang, W. Zheng, Q. Shen, et al., Identification and construction of a novel biomimetic delivery system of paclitaxel and its targeting therapy for cancer, Signal Transduct. Target. Ther. 6 (2021), 33.
[55] C. Hong, D. Wang, J. Liang, et al., Novel ginsenoside-based multifunctional liposomal delivery system for combination therapy of gastric cancer, Theranostics 9 (2019) 4437–4449.
[56] Y.W. Koh, S.J. Lee, S.Y. Park, Differential expression and prognostic significance of GLUT1 according to histologic type of non-small-cell lung cancer and its association with volume-dependent parameters, Lung Cancer 104 (2017) 31–37.
[57] Y. Weng, X. Fan, Y. Bai, et al., *SLC2A5* promotes lung adenocarcinoma cell growth and metastasis by enhancing fructose utilization, Cell Death Discov. 4 (2018), 38.
[58] Y. Zhu, J. Liang, C. Gao, et al., Multifunctional ginsenoside Rg3-based liposomes for glioma targeting therapy, J. Control. Release 330 (2021) 641–657.
[59] M. Wang, Y. Xu, J. Xie, et al., Ginsenoside as a new stabilizer enhances the transfection efficiency and biocompatibility of cationic liposome, Biomater. Sci. 9 (2021) 8373–8385.
[60] J. Xia, S. Ma, X. Zhu, et al., Versatile ginsenoside Rg3 liposomes inhibit tumor metastasis by capturing circulating tumor cells and destroying metastatic niches, Sci. Adv. 8 (2022), eabj1262.